

Research Paper

Segregation Effect on Solidification Cracking in Spot Welding of the 6XXX Aluminum

Andrés RAMIREZ¹⁾, Jonathan GRACIANO-URIBE²⁾
Diego HINCAPIE²⁾, Edwar TORRES^{1)*}

¹⁾ *Department of Mechanical Engineering
Research Group – GEA, Universidad de Antioquia
Medellín, Colombia*

*Corresponding Author e-mail: eandres.torres@udea.edu.co

²⁾ *Department of Mechatronic Engineering
Research Group – MATyER, Instituto Tecnológico Metropolitano
Medellín, Colombia*

Solidification cracking is a critical phenomenon, especially in the welding of AA6XXX, due these alloys present a wider freezing temperature range. The amount of liquid at the end of the solidification is a dominant factor in promoting or reducing the number of cracks. This paper proposes to assess the effect of the heat input in controlling the cracking during the spot welding in AA6061-T6. Four deposit conditions, made with GTAW, were assessed, in which the cracking degree was quantified and compared with the resulting microstructure. This work confirms and explains why the heat input governs the constitutional cooling, which simultaneously controls the microsegregation amount. With low heat input, the segregation is interdendritic, and the eutectic liquid gathers within the grains, which reduces the cracking susceptibility. A high heat input promotes the higher accumulation of eutectic liquid at the grain boundaries, facilitating cracks' formation and growth. A high concentration of eutectic liquid promotes the healing effect, reducing the formation of cracks.

Key words: constitutional supercooling; micro segregation; healing effect.

1. INTRODUCTION

Cracking during solidification is a serious problem in processes that involve the fusion and solidification of alloys, known in welding as solidification cracking [1], and in casting as hot tearing [2]. The generalized theory of cracking define that cracking takes place when a continuous liquid films separate the grains, and the local tensile stresses/strains overtake its strength to cracking [3]. Several

factors affect the solidification cracking susceptibility highlighting the solidification temperature range, the quantity of liquid at the end of solidification, the ductility of the weld metal, the degree of weld metal contraction, and the level of restraint [3]. An important feature is that cracking occurs in the mushy zone when the alloy tends to shrink and thermal contraction during solidification. CROSS and BÖLLINGHAUS [4] assume that the crack starts when the pressure in the interdendritic liquid drops, due to the inability to counter the solidification shrinkage and thermal contraction. Furthermore, ZHANG *et al.* [5] note that, an extensive the solidification temperature range produce a larger mushy zone, and more susceptibility to solidification cracking, promoting by the formation of long, and slim dendritic substructure, with lower fluid flow between the dendrites.

Several techniques have been developed for reducing or eliminating the solidification cracking [6]: the first one includes the use of a filler metal and welding conditions so that the weld metal reaches a composition away from the peak of the crack sensitivity curve. Another solution considers the formation of a small equiaxial dendritic structure with a large amount of liquid between grains, to promote the more easily deformation under stresses. An added alternative is the control of impurities, to avoid the formation of low-melting-point compounds, extending the solidification temperature range. Finally, is considered the formation of an adequate volume of liquid metal near the cracks to “backfill” and “heal” the developing cracks, where the restorative does not mean that the crack melts and heals, because what happens is that the eutectic promotes the sealing of the defect, preventing its subsequent growth [6].

In this sense, LIU *et al.* [7] explain that there are three types of dynamic cracking models in aluminum alloys: 1) aluminum alloys that have healing effect, in which it is possible to be free of cracks, such as ZL101 alloy; 2) those with deformation and breaking down of metal bridge, such as AA5083; and 3) the model where there is a separation of liquid film along grain boundary, such as AA6082, which has a higher susceptibility to solidification cracking.

Aluminum alloys with copper or magnesium result in unweldable alloys [8], attributed to the formation of a low melting Al-Cu-Mg eutectic. ARATA *et al.* [9] developed some of the first works for the characterization of the solidification cracking in many aluminum alloys. Using the Trans-Varestrain test, the authors measured the minimum augmented strain needed to cause cracking (E_{\min}) and the maximum crack length (L_{\max}) and quantified the brittleness temperature range (BTR), and the effect of the straining rate in the ductility of the weld metal [10]. ROSENBERG *et al.* [11] and CROSS *et al.* [12] observed less cracking during solidification for Al-Mg alloys than Al-Cu alloys, although it is expected a more susceptible the Al-Mg alloys because of their much more extensive solidification temperature range. To avoid cracking, welding wires of the type 4XXX

and 5XXX are used to modify the weld metal composition and the freezing range, taking it out of the crack-sensitive range [13–17].

The first model of hot tearing founded on physical principles, known as the RDG model, proposed by RAPPAZ *et al.* [18], defines a criteria based on the mass balance between the liquid and solid, where the perpendicular deformation to the growing dendrites are compensated by the interdendritic liquid feeding, considering a critical deformation rate beyond which the nucleation of a first void, occurs. As a complement to this model, KOU [19] developed a model focusing on the grain boundary and proposed an index for the susceptibility of an alloy to crack during solidification. This index is $|dT/d(f_S^{1/2})|$, where T is temperature and f_S the solid fraction in the semisolid region in the mushy zone. Thus, $|dT/d(f_S^{1/2})|$ near $(f_S)^{1/2} = 1$ shows a high cracking susceptibility. This model was proved successfully by LIU and KOU [20] in a very simple solidification cracking test, called the transverse motion weldability (TMW) test [21].

Aluminum alloys 6XXX are recognized to be prone to hot cracking, due to their high thermal expansion, large solidification shrinkage, and wide solidification temperature range [22–25], where the solidification shrinkage is caused by the higher density of the solid than the liquid [26]. Using the TMW test allowed to evaluate the effect of the filler metal on solidification cracking susceptibility of an AA6061, using 4043 and 4943 filler metal, and showing that the ER4943 was more effective [27]. In 6XXX series alloys, the main factor affecting this phenomenon is the amount of solute in the weld pool, being especially sensitive in alloys with elements between 0.8% and 6.0 %wt. [28]. The cracking in this case can be controlled in two ways: 1) by significantly raising the segregation to increase the amount of liquid with eutectic composition and be able to fill the spaces generated during the material shrinkage (healing), or 2) by significantly reducing the segregation, and therefore the amount of eutectic formed [29]. In autogenous welding processes, the bead composition does not change regarding the parent metal, increasing the crack risk during welding. For this reason, the use of filler metal to control the cracking has become a widespread practice. Nonetheless, with this solution, it is not clear which of the mechanisms implemented, increasing or reducing the eutectic [30]. The aim of this paper is to establish how the welding parameters affect the segregation degree, and with this, the hot cracking level of autogenous welding in AA6061-T6 aluminum alloys.

2. METHODOLOGY

Spot welds were made on a 1.85 mm AA6061-T6 aluminum alloy sheet, with the chemical composition presented in Table 1, determined by glow-discharge optical emission spectroscopy (GDOES).

Table 1. Chemical composition of the AA6061-T6 determined by GDOES (wt. %).

Si	Fe	Cu	Mn	Mg	Cr	Bal.
0.437	0.192	0.0054	0.0035	0.510	0.0017	98.79

The process used was autogenous gas tungsten arc welding (GTAW), along with 100% Ar gas protection. A support for the torch was built to ensure weld spots with a constant arc length of 5.0 mm, as shown in Fig. 1. The pulse was kept constant at 2.0 s, and the arc was started with the no-contact mode, commonly known as high frequency start.



FIG. 1. Torch support for keeping constant the arc length.

The spots welds were produced using four current levels, for which the nominal heat input (Q) was calculated based on the equation (2.1)

$$(2.1) \quad Q = \eta \cdot I \cdot V,$$

where V is voltage, I is current, and η is the process efficiency, where for GTAW is 0.7 [31]. The nominal heat input [W], which is a variant of the heat input per unit of length of weld [J/mm], makes it possible to relate the welding parameters with the amount of heat, punctual, introduced to the metal during the process. From this, it will be possible to relate the welding parameters with cracking and microstructure. Data are shown in Table 2. Sixteen samples were produced,

Table 2. The welding parameters used for the sample fabrication.

No.	Current* [A]	Voltage [V]	Heat input [W]
1	75	10	525
2	100	12	840
3	125	12	1.050
4	150	14	1.470

* DCEN.

four for each parameter. The cleanliness of the surface was guaranteed by means of a high frequency plasma, which works for 2.0 s before starting the welding arc. One sample from each parameter is randomly selected for the microstructural characterization using optical microscopy (OM) and scanning electron microscopy (SEM). The samples were polished using alumina of 0.3 μm , and then etched with fluor hydric acid at a concentration of 0.5% vol. The cracking degree is determined by the crack length measurement criterion, in terms of the total accumulated crack length (TLC), but the crack width was also considered as a criterion.

Lastly, a microhardness measure was conducted in the fusion line using a 50 g load and 15 s time ($\text{HV}_{0.5/15}$), with a spacing between each indentation of 100 μm , to determine the hardness both of the deposit and the weld pool. The measurement was taken 10 weeks after to allow the post-weld natural aging, which will be used as a sign of the amount of alloy elements remaining in the solid solution that will later provide the natural aging.

3. RESULTS AND DISCUSSION

The macrographs in Fig. 2 show the change in cracking with heat input. At low power, there are more cracks, but they are narrower. As the power increases, there are less cracks, but they are wider.

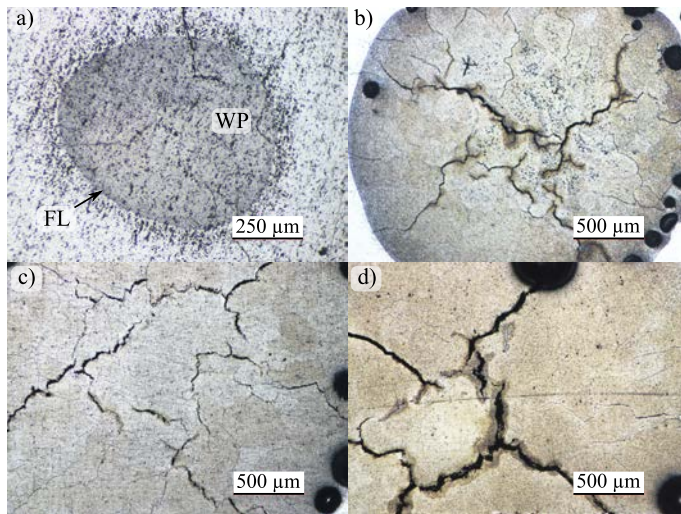


FIG. 2. MO images of the spot weld for the currents: a) 75 A, b) 100 A, c) 125 A, d) 150 A.

To evaluate the severity of the crack, the total accumulated crack length (TCL) [29] concept was used. The results are shown in Table 3. Clearly, the

Table 3. Total accumulated crack length (TCL) for each parameter of the spot welds.

Current [A]	TCL [μm]
75	2274 + 156
100	5234 + 274
125	7532 + 263
150	5833 + 387

quantity of cracks (TCL) increases with the welding current, but subsequently, their number decreases, although their width increases.

The higher number of cracks is found at a current of 125 A, but the most severe gap is seen at 150 A. At low current (> 75 A), the stress level can be low, so that it does not produce the formation of cracks; likewise, the size of the mushy zone is small, which allows healing of the voids formed. The least number of cracks seen in the 150 A sample could be explained as a consequence of a higher quantity of liquid at the end of the solidification, which would correspond to the first cracking control mechanism (healing). It is clear how for the different conditions, the size of the fusion zone changes significantly, as well as the degree of the hot cracking, where some cracks even growth through the mushy zone (MZ), the partial melting zone (PMZ) and the heat affected zone (HAZ), as shown in Fig. 3.

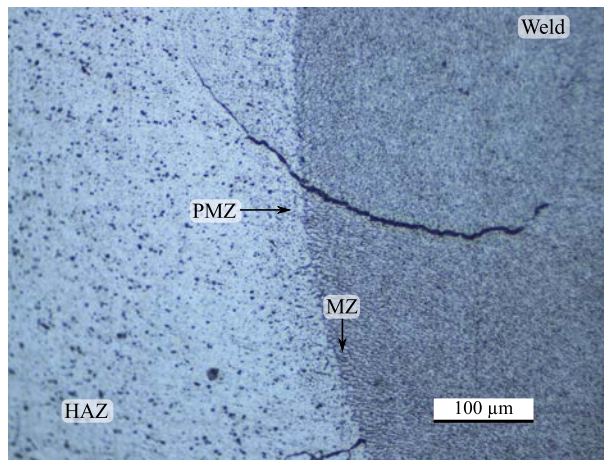


FIG. 3. OM micrograph of the spot weld produced at 125 A, showing the spread of the crack through the mushy zone (MZ), partial melting zone (PMA), and HAZ.

Cracks spread in radial direction, due the form of the weld pool. As expounded by ZHANG *et al.* [32], in spot welding the melted metal is surrounded

by the solid metal, which produces tensile stresses in the heat affected zone (HAZ), nearly tangent of the isotherm near the fusion zone. For this reason, the orientation of cracks is normal to the direction of maximum tension. In welding, as the current increases, the metal pool size rise (Fig. 4a), and with this, the intensity of the stresses on to the molten metal, which could explain the increment in the severity of the cracking when it is seen as a criterion for the crack spacing.

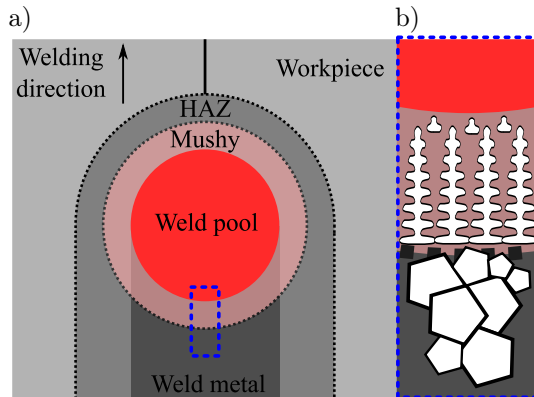


FIG. 4. a) Effect of constitutional supercooling on solidification mode and the size of the mushy zone, adapted from [3]; b) weld pool diagram and columnar substructure formation in the mushy zone, adapted from [21].

Furthermore, welding parameters are also responsible for the size variation of the mushy zone, thus, an extended mushy zone increases solidification cracking susceptibility [3]. The increasing in the constitutional supercooling generates an extended two-phase mushy zone (Fig. 4a), where the temperature gradient (G) controls the cell or dendrite length (l_c) in the mushy zone, such length is determined by

$$(3.1) \quad l_c = \frac{\Delta T'}{G} = \frac{(T^* - T'_s)}{G},$$

where $\Delta T'$ is the difference in temperature between the cell or dendrite tip (T^*) and the root temperature (T'_s), and G is the temperature gradient [5]. The measurement of these variables is carried out using numerical simulation from metals' properties and the determination of the temperature at various points of the sample [33–35]. Therefore, the increase in current generates a larger weld pool, which reduces the temperature gradient (G), and increases the constitutional supercooling, and the size of the mushy zone, and with this, the length of cells or dendrites.

Several models claim that a wide mushy zone will suffer more shrinkage strain, therefore, will be more susceptible to cracks [36]. Hence, the welding of

a susceptible alloy employing high heat input (i.e. low G), increase the chance of cracking [37]. These occur because as the l_c increases, dendrites size also grows, favoring the increase of the residual stresses.

Another theory establishes that extended dendrites (larger mushy zone), hinder the feeding between dendrites, due to difficulty for the liquid metal to reach a deeper cavity (Fig. 4b).

In the case of the spot weld, the mushy zone, as the partially melted zone, surrounds the weld pool (Fig. 5a). Regarding the parameters evaluated, the Fig. 5 shows that there is a cellular substructure in the mushy zone. This means there is a low constitutional supercooling and a high G/R . This happens when G is high, which is inversely proportional to the weld pool. Therefore, the mushy zone presents a cellular structure for all the conditions evaluated, which means that the cracking does not affect that region. This happens more towards the center of the weld spot, where the resulting structure is dendritic. As explained by APOLINARIO *et al.* [38], the microstructure in the fusion zone is determined by the change in the solidification parameter (G/R), as shown in Fig. 5a.

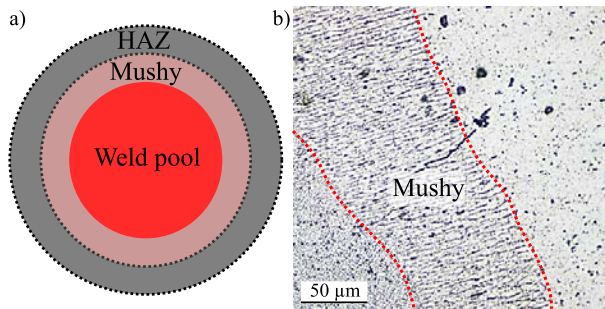


FIG. 5. a) Diagram of the weld pool in the weld tack and b) microstructure in the mushy zone mushy showing the cellular structure formation.

The presence of cells in the fusion line is because G/R is at a maximum at the boundary and decreases at the center of the pool, indicating that the presence of dendrites would be expected. As the welding current increases, the weld pool grows, reducing G , which promotes a higher formation of dendrites, increasing crack susceptibility. ZHANG *et al.* [5] agree with this view of the phenomenon. They explain that changes in welding parameters can noticeably alter the cooling rate, solid/liquid interface rate (R), the temperature gradient in the liquid (G), and micro segregation. These changes will promote the alteration in solidification temperature range, and dendrite growth rate, which consequences in the microstructural features as mushy zone width, dendrite arm spacing, and cell or cellular dendrite length. All of these factors ultimately affect the susceptibility to solidification cracking in 6061-T6 aluminum [5].

Hence, the presence of cells in the fusion line (Fig. 5b) is associated with the formation of a narrower mushy zone; due to its shorter length (l_c), the cells allow the liquid metal to reach the intercellular spacing (healing), reducing the crack formation susceptibility. Clearly, most of the cracking is not originated in the mushy zone but towards the weld pool.

A more detailed analysis, shown in Fig. 6, shows the microstructure and the surface of the cracks, where the dendritic growth is observed, as well as the presence of the intermetallic compounds (IMC, white) in the dendritic arms, as a result of the micro segregation during solidification. In Fig. 6b, it is even possible to identify the growth of the dendrites on the crack surface.

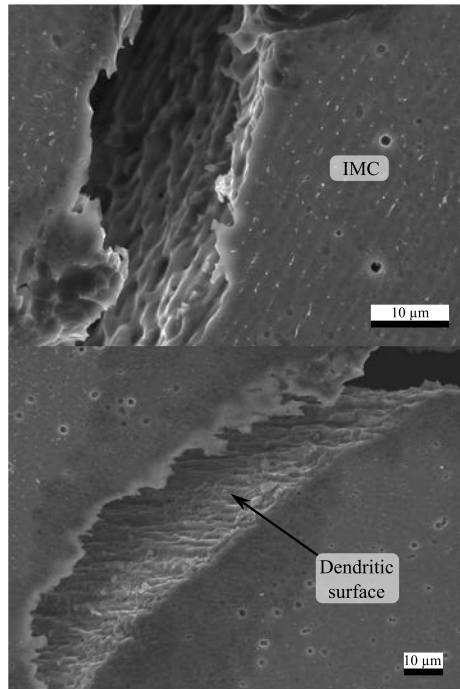


FIG. 6. Micrographics by SEM of the welding spots showing the presence of IMC and dendritic growth: a) weld tack produced at 125 A and b) 150 A.

In aluminum alloys of series 6XXX are possible the formation of eutectics with low-melting-point, such as Al-Mg₂Si, Al-Si, where its melting temperature of 868 K [39] is lower than the liquidus temperature of 6061-T6 (925 K) [40]. The continuous solute enrichment of liquid film and the formation of such eutectics will increase the solidification range and the susceptibility to solidification cracking in such alloys [5].

The amount of segregation in the weld pool can be quantified using different methods. This paper, nonetheless, will use a qualitative evaluation regarding

the effect of the welding current in the generation of segregation, by means of the micro-hardness measurement in the weld pool. Results for the different conditions evaluated are shown in Fig. 7. Comparing hardness to segregation is possible if one takes into consideration that during solidification, most of the alloy elements used for the formation of the $\text{Mg}_2\text{Si}''$ (β''), which is the element responsible for the tensile strength of the AA6XXX alloys [41–43], are trapped in form of segregation. During equilibrium solidification of these alloys, the solute is dissolved in the matrix of aluminum grains, hardening the metal by the solid solution mechanism. However, in the welding process, constitutional supercooling breaks the solid/liquid interface, segregating the solute to the boundaries between cells or dendrites. At higher constitutional cooling, more significant will be the quantity of elements segregated. Therefore, the structure loses solute, reducing its hardness due to the solid solution hardening mechanism. This implies that when microhardness is performed, the microstructure is softer, since more elements were converted into segregation. At lower hardness, less amount of segregation is expected, since the amount of Al-Mg₂Si eutectic will decrease.

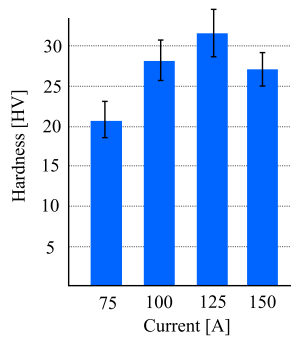


FIG. 7. Vickers hardness within the weld zone, where the hardness of the AA6061-T6 base metal is 107 HV.

The progressive increase in the current produces a hardness increment, which would be associated with a higher presence of eutectics. Likewise, there is an augmentation in the cracking, as shown in Table 3, where the higher TCL is seen in the sample produced at 125 A, which also coincides with the highest hardness reached. Both phenomena would be associated with the presence of low-melting-point eutectics in the fusion zone.

In the samples produced at low current, the presence Mg_2Si would be observed mainly in the form of interdendritic micro segregation, which is lower in comparison to the intergranular micro segregation. The former is due to the accumulation of solute in the interdendritic arms of the solidified structure, while the latter is due to the accumulation of solute between the grains formed by the dendrite packages, as shown in Fig. 5a. Figure 2 clearly shows how the cracking

is produced near the grain boundaries, where the amount of solute-rich fluid would be much higher, favored by the dendrite packages, which generate a more elevated peak of chemic composition when the grains find each other.

The segregation control during solidification depends on the solute distribution during the progress of the solid/liquid interface. Segregation is the result of constitutional supercooling by the accumulation of solute in the front of the solidification [28]. The kind of substructure generated by the breaking of the interface: cellular, columnar dendritic, or equiaxial, depends on the degree of constitutional supercooling between the substructures, which also generates a higher or lower accumulation of solute in the form of micro segregation.

The amount and chemical composition of the intergranular liquid is determined by the constitutional supercooling. As shown in Fig. 8, the severity of the constitutional supercooling increases as the solidification parameter (G/R) decreases; for this reason, as the electric current increases, the weld spot increases as well, reducing G . In turn, since the size of the mushy zone is bigger, the speed of the solid growth (R) increases, and the combination G/R decreases. This explains the formation of bigger dendrites. This higher speed promotes the formation of bigger and bigger grains (Fig. 2), which move a greater amount of solute, which in turns promotes the formation of eutectic liquid.

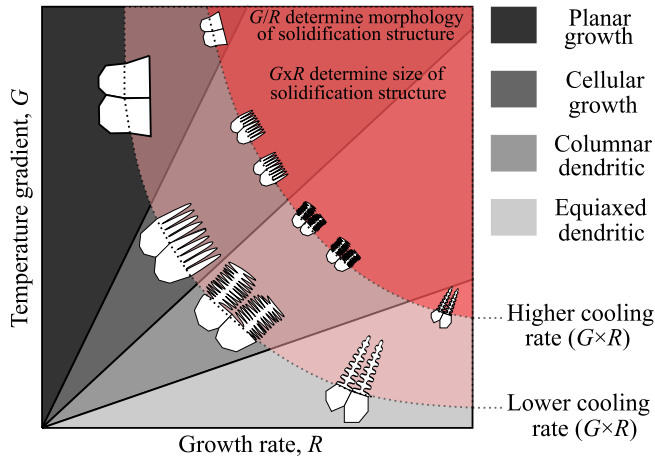


FIG. 8. Effect of temperature gradient (G) and growth rate (R) on the morphology and size of solidification microstructure. Adapted from [3].

It is known that a significant reduction of G/R can produce equiaxial dendrites, which indicate lower cracking susceptibility, due to the fact that the surrounding liquid is subject to lower stresses, since this structure is more flexible, adjusting easily to the volumetric change during solidification. This is not the case for the sample produced at 150 A, where the high Q significantly reduced

the TCL; not because of the presence of equiaxial dendrites, but because of the significant increment in the amount of eutectic liquid, which allowed the healing in smaller cracks.

In a simpler way: a lower nominal heat input (Q) increases the G/R , where the higher segregation is interdendritic, which reduces the TLC. An increment in Q generates a reduction in the G/R , thus, the interangular segregation increases, increasing also the cracking. A significant increment in the Q promotes a very high G/R , which results in the formation of a great amount of eutectic liquid, producing healing.

4. CONCLUDING REMARKS

This study was focused on establishing the effect of spot weld parameters on segregation and its relationship to solidification cracking in AA6061 alloy. The conclusions obtained from this study are presented below. The number of cracks (TCL) increases with the welding current, but subsequently, their number decreases, although their width increases. This occurs because at very low current the stress level can be low and the size of the mushy zone is small, allowing the healing of the voids. The reduction of the number of cracks at high current could be explained as a consequence of a higher quantity of liquid at the end of the solidification, filling the smaller cracks.

The development of cellular structure hinders solidification cracks and failures are formed towards the center of the weld spot, where the resulting structure is dendritic. The mushy zone size is a fundamental parameter to determine the susceptibility to cracking, because it controls the length of the solidification substructure (cellular or columnar dendrites), favors or hinders the feeding between dendrites, and hence, makes it difficult for the liquid metal to reach a deeper cavity.

The segregation control during solidification depends on the solute distribution during the progress of the solid/liquid interface. It was possible to show how the heat input determines the constitutional supercooling degree, which directly controls the shape and amount of microsegregation. With low heat input, segregation is interdendritic, that is, the eutectic liquid concentrates within the grains, reducing the possibility of cracking. A high heat input could result in a great amount of eutectic liquid, which allows the healing effect to reduce the crack formation.

ACKNOWLEDGEMENTS

To the Metallography laboratory of the University of Antioquia for allowing the metallographic preparation and the hardness measurements. To the GIPIME

group for allowing the use of the optic microscope. To the Electronic Microscopy laboratory for facilitating the characterization through SEM. To our colleagues José Julian Rúa y Jhonathan Alfonso Salazar, Mechanic Engineering students at the University of Antioquia, for their support in the experimental development.

REFERENCES

1. CLYNE T.W., WOLF M., KURZ W., The effect of melt composition on solidification cracking of steel, with particular reference to continuous casting, *Metallurgical Transactions B*, **13**(2): 259–266, 1982, doi: 10.1007/BF02664583.
2. CAMPBELL J., *Castings*, Elsevier, 2003.
3. KOU S., Solidification and liquation cracking issues in welding, *JOM*, **55**(6): 37–42, 2003, doi: 10.1007/s11837-003-0137-4.
4. CROSS C.E., BOELLINGHAUS T., The effect of restraint on weld solidification cracking in aluminium, *Welding in the World*, **50**(11–12): 51–54, 2006, doi: 10.1007/BF03263461.
5. ZHANG J., WECKMAN D.C., ZHOU Y., Effects of temporal pulse shaping on cracking susceptibility of 6061-T6 aluminum Nd:YAG laser welds, *Welding Journal*, **87**(1): 18–30, 2008.
6. KOU S., Weld metal solidification cracking, [in:] *Welding Metallurgy*, New Jersey: John Wiley & Sons, Inc., pp. 263–295, 2003, doi: 10.1002/0471434027.ch11.
7. LIU R., DONG Z., PAN Y., Solidification crack susceptibility of aluminum alloy weld metals, *Transactions of Nonferrous Metals Society of China*, **16**(1): 110–116, 2006, doi: 10.1016/S1003-6326(06)60019-8.
8. CROSS C., KRAMER L., TACK Q., LOECHEL L., Aluminum weldability and hot tearing theory, [in:] *Welding of Materials ASM Int.*, pp. 275–282, 1990.
9. ARATA Y., MATSUDA F., NAKATA K., SASAKI I., Solidification crack susceptibility of aluminium alloy weld metals (Report I): Characteristics of ductility curves during solidification by means of the trans-varestraint test, *Trans. JWRI*, **5**(1976–12): 153–167, 1983.
10. ARATA Y., MATSUDA F., NAKATA K., SHINOZAKI K., Solidification crack susceptibility of aluminum alloy weld metals (Report II): Effect of straining rate on cracking threshold in weld metal during solidification, *Trans. JWRI*, **6**(1977–06): 91–104, 1983.
11. ROSENBERG R.A., FLEMINGS M.C., TAYLOR H.F., Nonferrous Binary alloys hot tearing, *AFS Transactions-American Foundry*, **68**: 518–528, 1960.
12. CROSS C.E., OLSON D.L., Hot tearing model to assess aluminum weldability, *Aluminium Alloys – Their Physical and Mechanical Properties*, **III**, pp. 1869–1875, 1986.
13. DUDAS J.H., Preventing weld cracks in high strength aluminum alloys, *Welding Journal*, **45**: 3, 1966.
14. OLSON D.L., SIEWERT T.A., LIU S., EDWARDS G.R., *Metals Handbook*, Vol. 6, *Welding Brazing and Soldering*, ASM Int. Mater. Park, 1990.
15. ZHAO H., WHITE D.R., DEBROY T., Current issues and problems in laser welding of automotive aluminium alloys, *International Materials Reviews*, **44**(6): 238–266, 1999, doi: 10.1179/095066099101528298.

16. LUIJENDIJK T., Welding of dissimilar aluminium alloys, *Journal of Materials Processing Technology*, **103**(1): 29–35, 2000, doi: 10.1016/S0924-0136(00)00415-5.
17. CAO X., WALLACE W., IMMARIGEON J.-P., POON C., Research and progress in laser welding of wrought aluminum alloys. II. Metallurgical microstructures, defects, and mechanical properties, *Materials and Manufacturing Processes*, **18**(1): 23–49, 2003, doi: 10.1081/AMP-120017587.
18. RAPPAZ M., DREZET J.-M., GREMAUD M., A new hot-tearing criterion, *Metallurgical and materials transactions A*, **30**(2): 449–455, 1999, doi: 10.1007/s11661-999-0334-z.
19. KOU S., A criterion for cracking during solidification, *Acta Materialia*, **88**: 366–374, 2015, doi: 10.1016/j.actamat.2015.01.034.
20. LIU J., KOU S., Crack susceptibility of binary aluminum alloys during solidification, *Acta Materialia*, **110**: 84–94, 2016, doi: 10.1016/j.actamat.2016.03.030.
21. SOYSAL T., KOU S., A simple test for assessing solidification cracking susceptibility and checking validity of susceptibility prediction, *Acta Materialia*, **143**: 181–197, 2018, doi: 10.1016/j.actamat.2017.09.065.
22. CIESLAK M.J., FUERSCHBACH P.W., On the weldability, composition, and hardness of pulsed and continuous Nd:YAG laser welds in aluminum alloys 6061, 5456, and 5086, *Metallurgical Transactions B*, **19**(2): 319–329, 1988, doi: 10.1007/BF02654217.
23. NAKATA K., MATSUDA F., Evaluations of ductility characteristics and cracking susceptibility of Al alloys during welding (materials, metallurgy & weldability), *Transactions of JWRI*, **24**(1): 83–94, 1995.
24. ÇAM G., KOÇAK M., Progress in joining of advanced materials, *International Materials Reviews*, **43**(1): 1–44, 1998, doi: 10.1179/imr.1998.43.1.1.
25. ION J.C., Laser beam welding of wrought aluminium alloys, *Science and Technology of Welding and Joining*, **5**(5): 265–276, 2000, doi: 10.1179/136217100101538308.
26. FLEMINGS M.C., *Solidification Processing*, McGraw-Hill Series in Material Science and Engineering, McGraw-Hill, New York, 1974.
27. SOYSAL T., KOU S., Effect of filler metals on solidification cracking susceptibility of Al alloys 2024 and 6061, *Journal of Materials Processing Technology*, **266**: 421–428, 2019, doi: 10.1016/j.jmatprotec.2018.11.022.
28. KOU S., LE Y., Nucleation mechanism and grain refining of weld metal, *Welding Research, Supplement to welding Journal*, **65**(4): 305–313, 1986.
29. BÖLLINGHAUS T., HEROLD H., CROSS C.E., LIPPOLD J.C., *Hot Cracking Phenomena in Welds II*. Springer Science & Business Media, 2008.
30. O'BRIEN A., GUZMAN C., *Welding Handbook: Welding Processes*, American Welding Society, 2007.
31. DUPONT J.N., MARDER A.R., The effect of welding parameters and process type on arc and melting efficiency is evaluated, *Welding Journal Including Welding Research Supplement*, **74**(12): 406–416, 1995.
32. ZHANG H., SENKARA J., WU X., Suppressing cracking in resistance welding AA5754 by mechanical means, *Journal of Manufacturing Science and Engineering*, **124**(1): 79–85, 2002, doi: 10.1115/1.1418693.

33. LU S.P., DONG W.C., LI D.Z., LI Y.Y., Numerical simulation for welding pool and welding arc with variable active element and welding parameters, *Science and Technology of Welding and Joining*, **14**(6): 509–516, 2009, doi: 10.1179/136217109X441182.
34. VEMANABOINA H., AKELLA S., BUDDU R.K., Welding process simulation model for temperature and residual stress analysis, *Procedia Material Science*, **6**: 1539–1546, 2014, doi: 10.1016/J.MSPRO.2014.07.135.
35. HOSSEINI V.A. *et al.*, A novel arc heat treatment technique for producing graded microstructures through controlled temperature gradients, *Materials & Design*, **121**: 11–23, 2017, doi: 10.1016/J.MATDES.2017.02.042.
36. CROSS C.E., OLSON D.L., Hot tearing model to assess aluminum weldability, [in:] *Aluminum Alloys – Their Physical and Mechanical Properties*, pp. 1869–1875, 1986.
37. CROSS C.E., On the origin of weld solidification cracking, [in:] *Hot Cracking Phenomena in Welds*, Berlin/Heidelberg: Springer-Verlag, pp. 3–18, 2008.
38. APOLINARIO L.H.R. *et al.*, Predominant solidification modes of 316 austenitic stainless steel coatings deposited by laser cladding on 304 stainless steel substrates, *Metallurgical and materials transactions A*, **50**(8): 3617–3628, 2019, doi: 10.1007/s11661-019-05293-y.
39. HATCH J.E., Metallurgy of heat treatment and general principles of precipitation hardening, [in:] *Aluminum: Properties and Physical Metallurgy*, J.E. Hatch [Ed.], pp. 134–159, ASM International, 1984, doi: 10.1361/appm1984p134.
40. LAMPMAN S., ZORE T.B., Wrought titanium and titanium alloys, [in:] *ASM Handbook, Vol. 2: Properties and Selection: Nonferrous Alloys and Special-Purpose Materials*, pp. 592–633, ASM International: Cleveland, OH, USA, doi: 10.31399/asm.hb.v02.9781627081627.
41. ZHANG J., FAN Z., Y. WANG Q., ZHOU B.L., Equilibrium pseudobinary Al-Mg₂Si phase diagram, *Materials Science and Technology*, **17**(5): 494–496, 2001, doi: 10.1179/026708301101510311.
42. WARMUZEK M., Metallographic techniques for aluminum and its alloys, [in:] *Metallography and Microstructures*, *ASM Handbook*, Vol. 9, G.F. Vander Voort [Ed.], pp. 711–751, ASM International, 2004, doi: 10.31399/asm.hb.v09.a0003769.
43. ARBELÁEZ J., HINCAPIÉ D.A., TORRES E., RAMÍREZ A.J., Characterization of AA6063-T5 aluminum alloy by optical microscopy, scanning electron and transmission electron [in Spanish], *Revista Colombiana De Materiales* (5): 59–64, 2014, <https://revistas.udea.edu.co/index.php/materiales/article/view/19131>.

Received April 29, 2020; accepted version September 22, 2020.

Published on Creative Common licence CC BY-SA 4.0

